Heterojunction interfacial promotion of fast and prolonged alkali-ion storage of urchin-like Nb_2O_5@C nanospheres

Zhipeng Zhao[a,b], Jingyun Cheng[a,b], Kai Li[a,b], Chuanqi Li[a,b], Shuo Zhang[c], Xiangdong Pei[d], Zhulin Niu[a,b]*, Zhongyi Liu[a,b], Yongzhu Fu[a,b] and Dan Li[a,b]*

[a] College of Chemistry, Zhengzhou University, Zhengzhou, Henan Province, 450001, P. R. China

[b] Green Catalysis Center, Zhengzhou University, Zhengzhou, Henan Province, 450001, P. R. China

[c] School of Nuclear Science and Technology, Lanzhou University, Lanzhou, Gansu Province, 730000, P. R. China

[d] Shanxi Supercomputing Center, Lvliang, Shanxi Province, 033000, P. R. China

*Corresponding authors

E-mail: danli@zzu.edu.cn; niuzhl@zzu.edu.cn

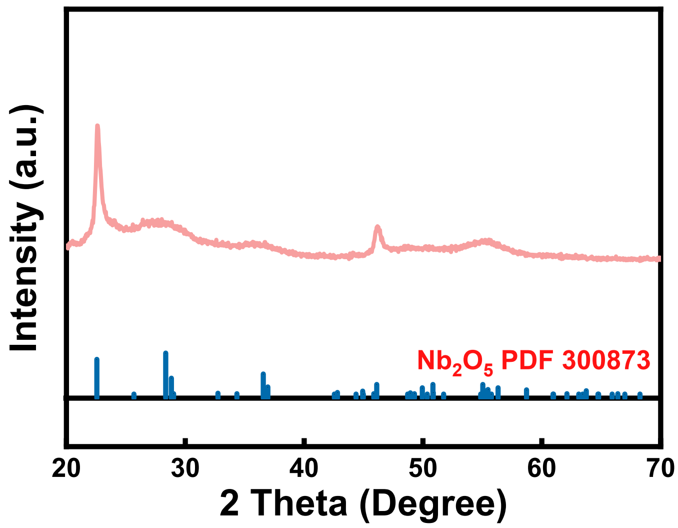

Fig. S1. The XRD pattern of the intermediate material obtained after the hydrothermal reaction, which is index to Nb_2O_5 (PDF card no. 300873).

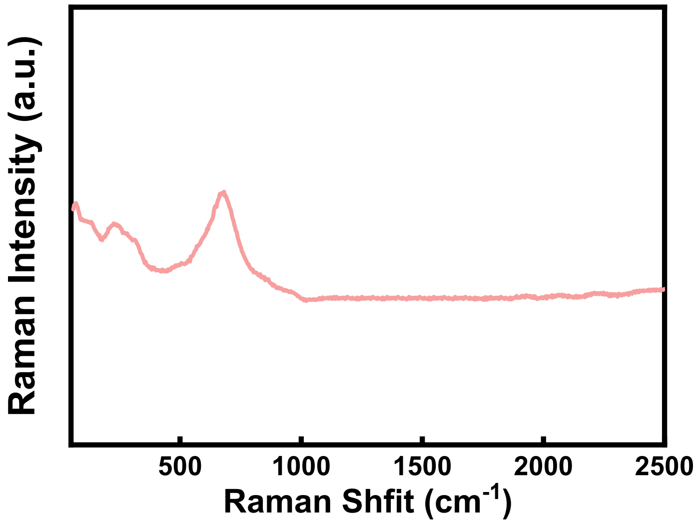

Fig. S2. The Raman spectrum of the intermediate material obtained after the hydrothermal reaction.

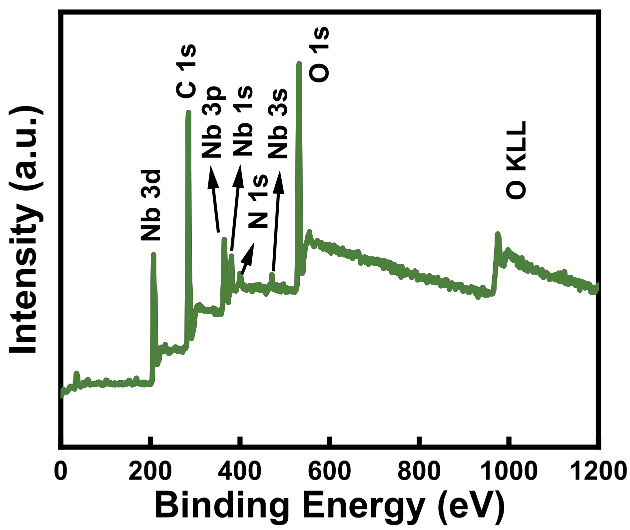

Fig. S3. Survey XPS spectrum of Nb_2O_5@C.

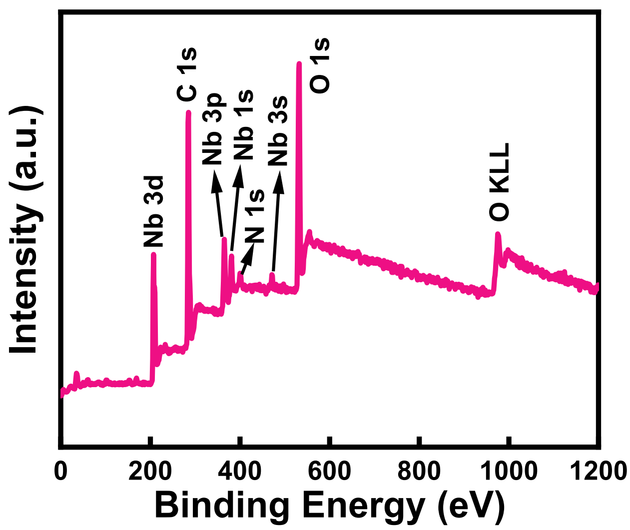

Fig. S4. Survey XPS spectrum of the bare Nb_2O_5.

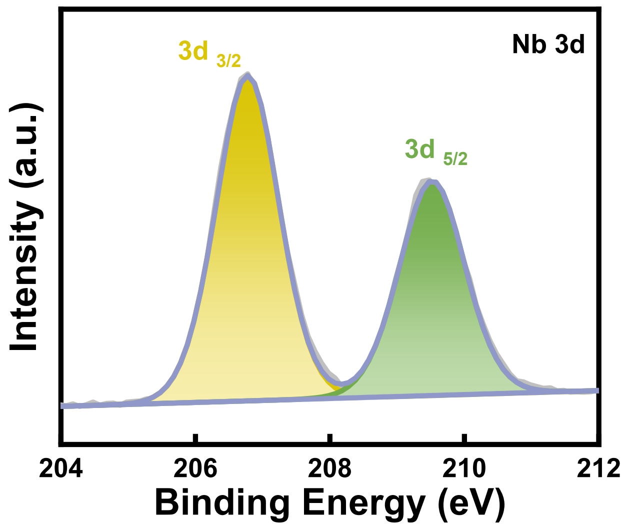

Fig. S5. High-resolution XPS spectrum of Nb 3d in the bare Nb_2O_5.

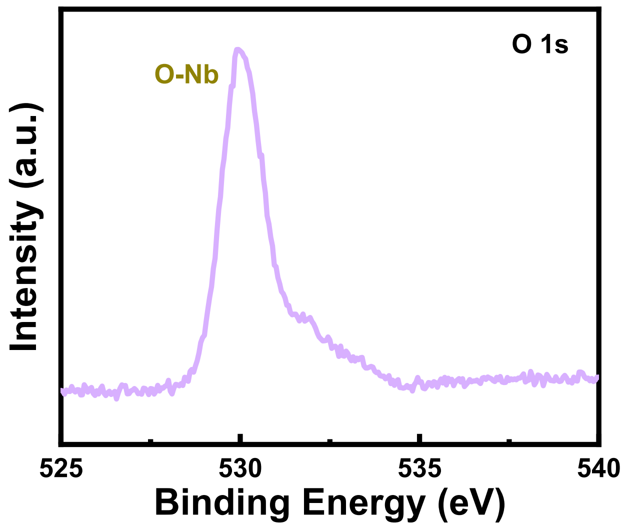

Fig. S6. High-resolution XPS spectrum of O 1s in the bare Nb_2O_5.

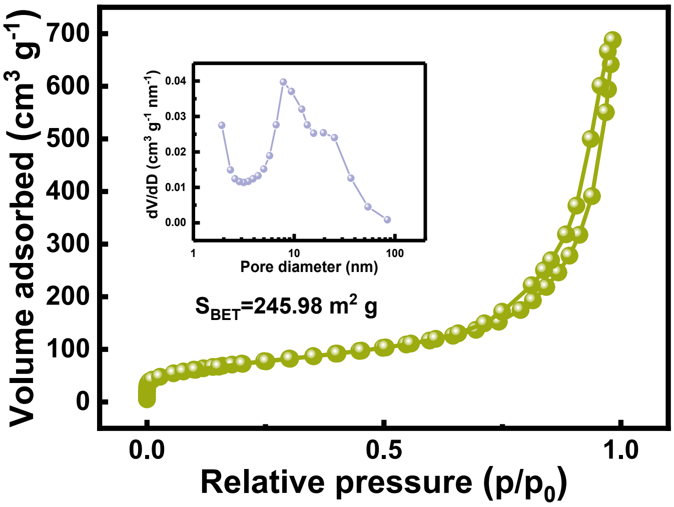

Fig. S7. Nitrogen sorption isotherms of the bare Nb_2O_5.

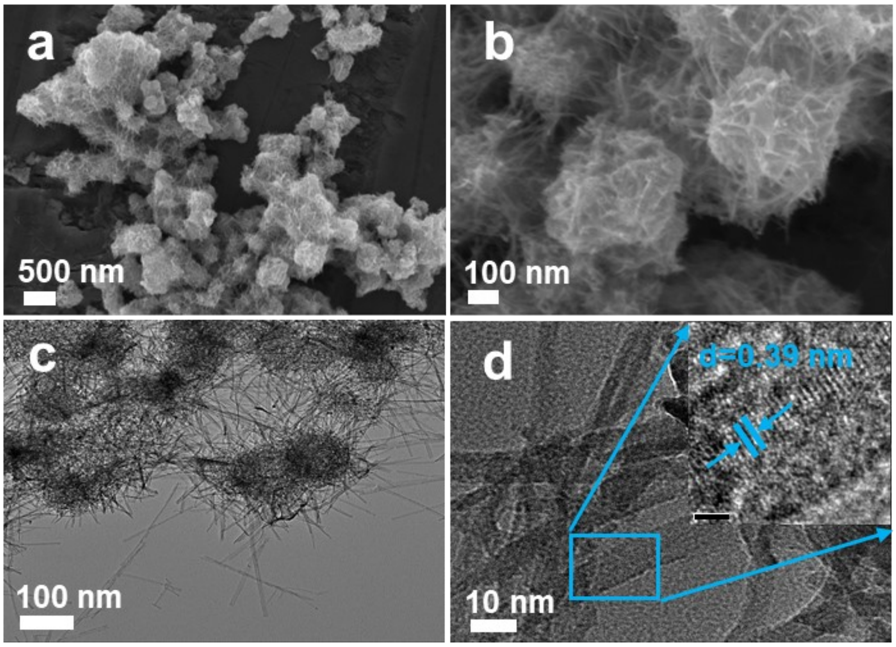

Fig. S8. a, b) SEM images and c, d) TEM images of the intermediate material obtained after the hydrothermal reaction.

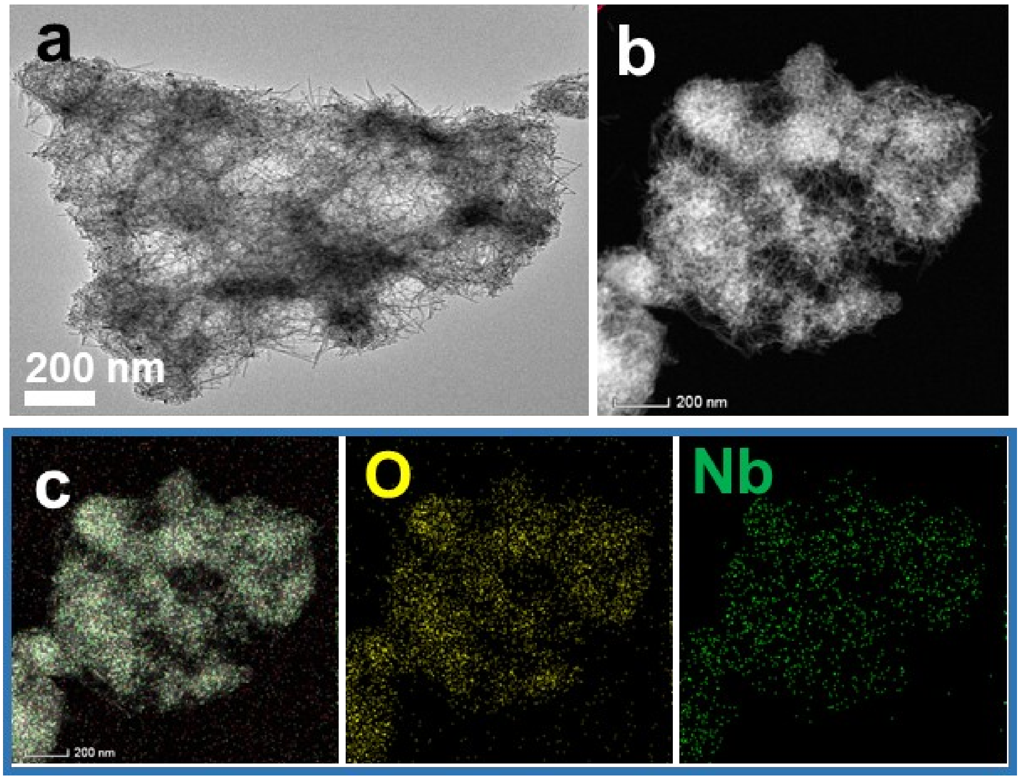

Fig. S9. (a) TEM image, (b) the HAADF image, and (c) elemental mapping images of O and Nb in the bare Nb_2O_5.

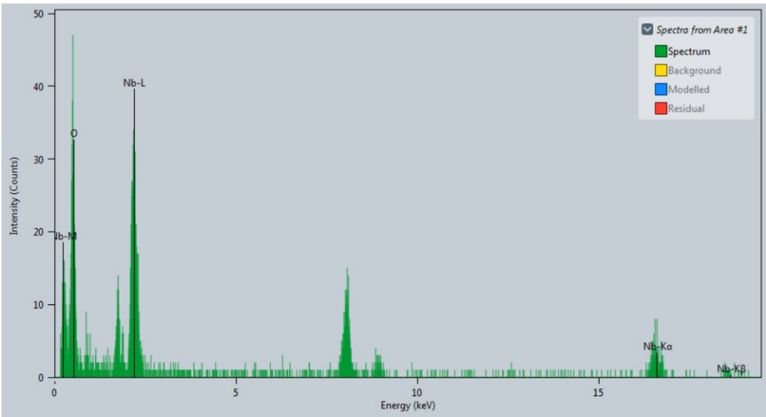

Fig. S10. The EDS of the bare Nb_2O_5 sample.

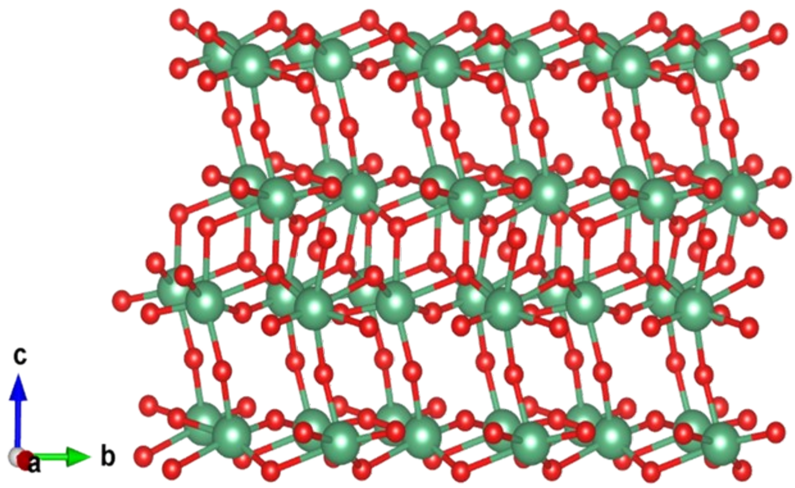

Fig. S11. The crystal structure of Nb_2O_5.

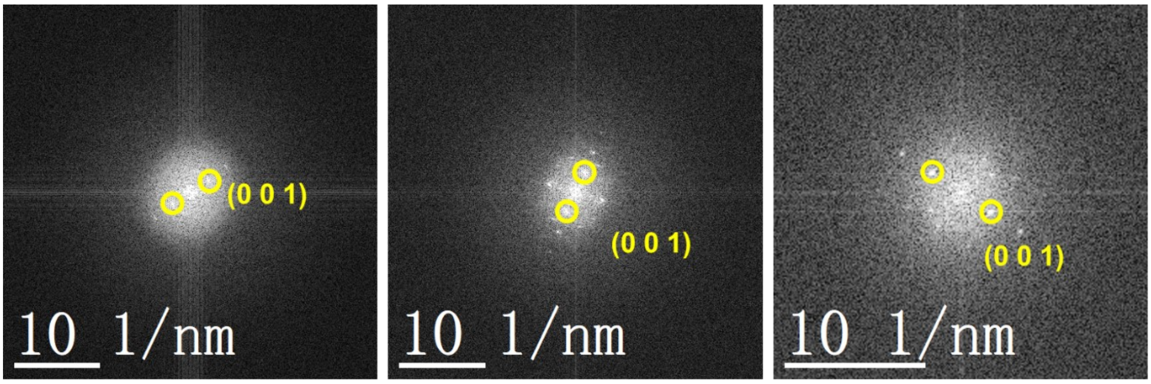

Fig. S12. The FFT diffraction pattern of obtained samples: a) the intermediate, b) bare Nb_2O_5 and c) Nb_2O_5@C.

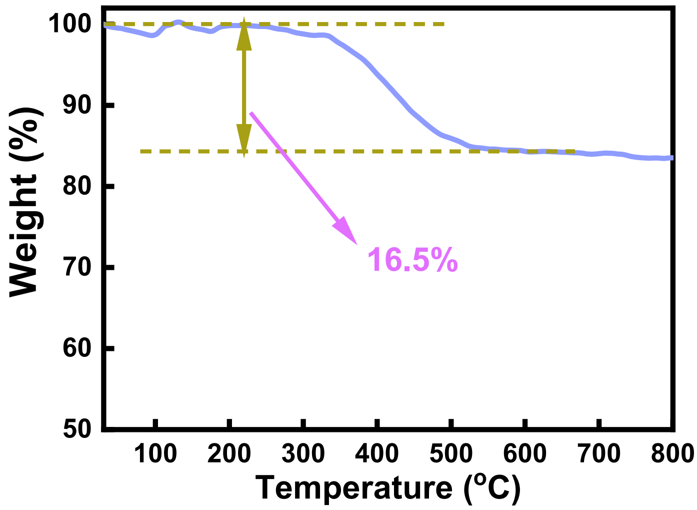

Fig. S13. The TG curve of Nb_2O_5@C.

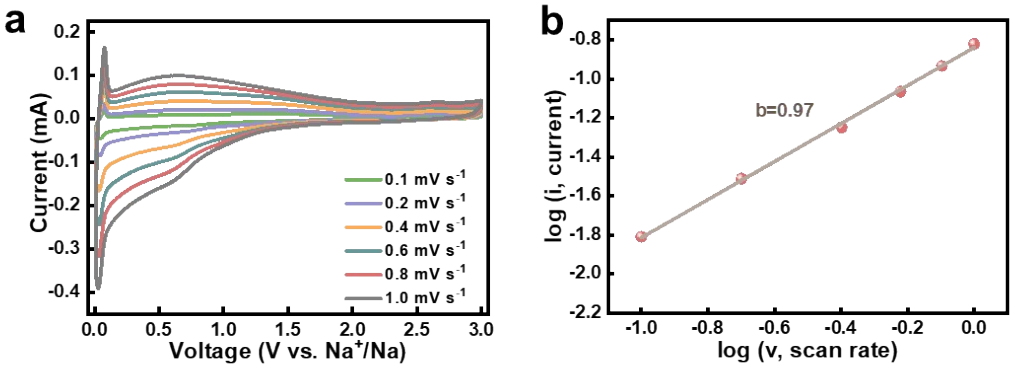

Fig. S14. a) CV curves at various scan rates, b) relationship between the peak currents and scan rates in logarithmic format of the Nb_2O_5@C composite in SIBs.

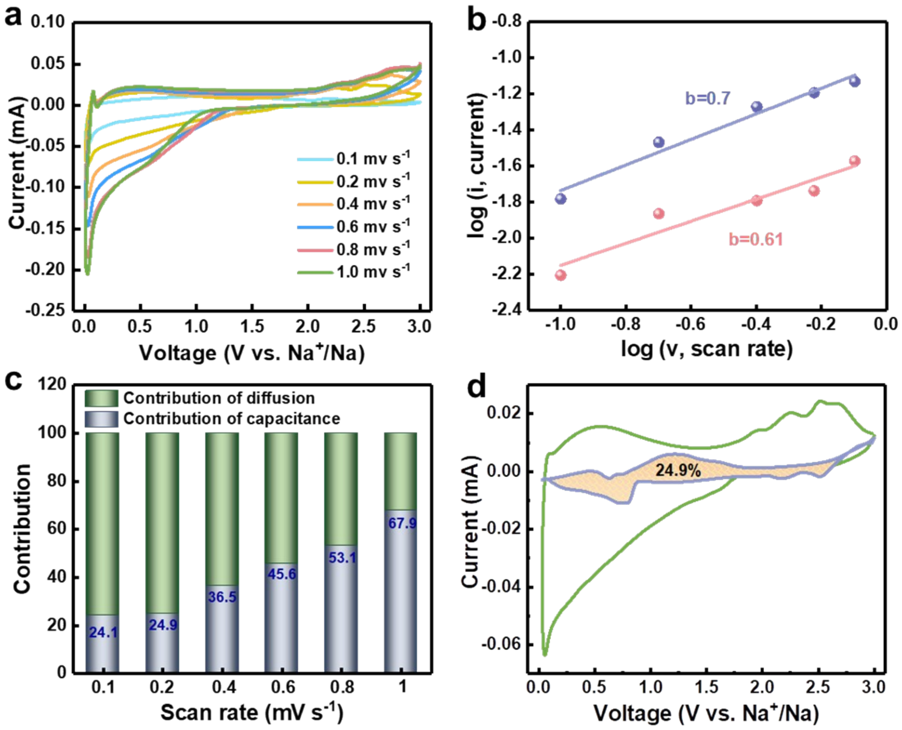

Fig. S15. Sodium-storage properties of the bare Nb_2O_5 in half-cells: a) CV curves at various scan rates, b) relationship between the peak currents (anodic and cathodic peaks) and scan rates in logarithmic format, c) contribution ratios of the capacitive and diffusion-controlled behaviors, d) capacitive contribution (shaded area) in a CV curve at 0.2 mV s^{-1}.

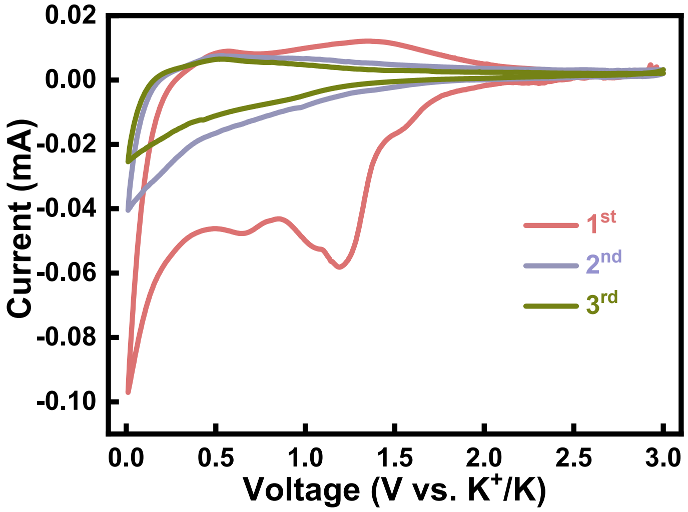

Fig. S16. CV curves of bare Nb_2O_5 at the scan rate of 0.1 mV s^{-1} between 0.01 and 3 V in the PIBs.

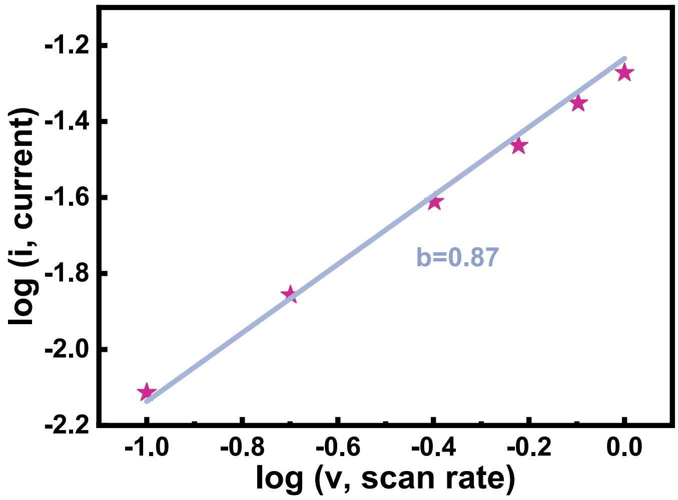

Fig. S17. Relationship between the peak currents and scan rates in logarithmic format of the Nb_2O_5@C composite in PIBs.

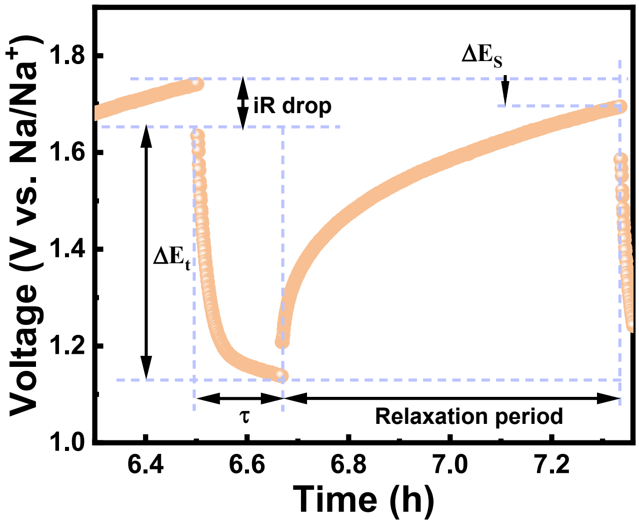

Fig. S18. *E vs. t* curve of the Nb_2O_5@C composite for a single GITT during discharge process.

The sodium diffusion coefficient (D_{Na^+}) can be calculated using the following equation:

$$D = \frac{4}{\pi\tau}\left(\frac{mV_m}{M_A S}\right)^2\left(\frac{\Delta E_S}{\Delta E_\tau}\right)^2$$

Where τ (s), m (g), V_m (cm^3 mol^{-1}), M_A (g mol^{-1}) and S (cm^2) are constant current pulse time, the active mass of electrode materials, molar volume of the active material, molecular weight and the effective surface area, respectively. And ΔE_s (V) presents the difference in the steady state potential of the step at plateau, while ΔE_τ (V) is the total voltage change during a constant current pulse time excluding the *iR* drop as depicted in Fig. S18.

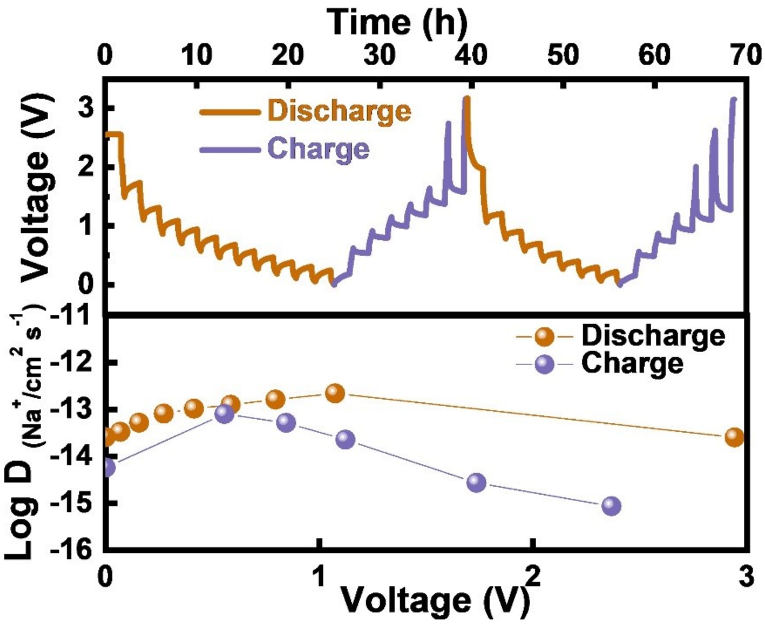

Fig. S19. The GITT curves and D_{Na^+} values at different discharge/charge states at the second cycle of bare Nb_2O_5 in sodium ion battery.

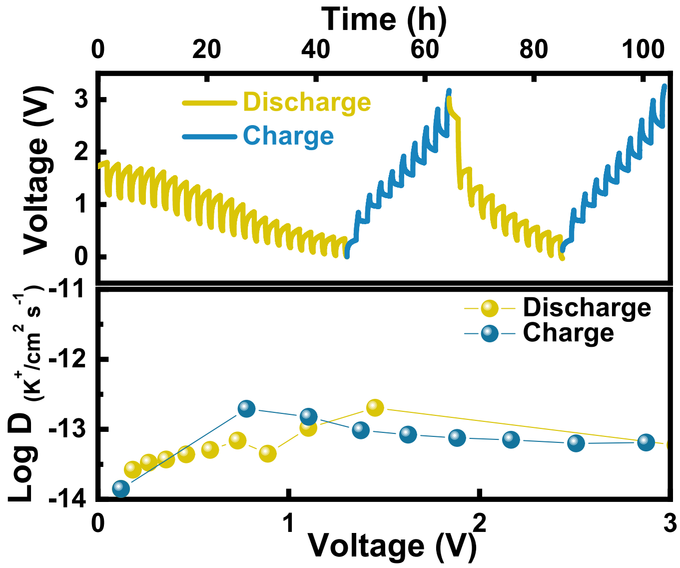

Fig. S20. The GITT curves and D_{K^+} values at different discharge/charge states at the second cycle of bare Nb_2O_5 in potassium ion battery.

It can be found that the D_{K^+} values of Nb_2O_5@C at charge/discharge process are higher than that of bare Nb_2O_5 whether in SIBs system or PIBs system, indicating the promoted ionic reaction kinetics stemmed from the rich high chemical activity of pyridinic N.

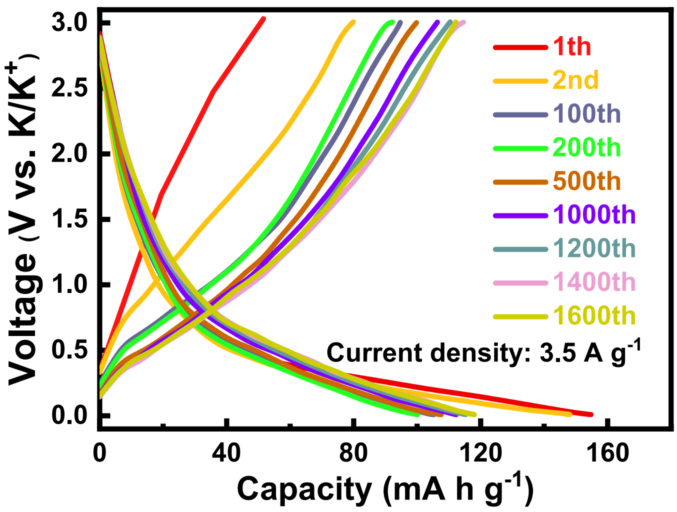

Fig. S21. Galvanostatic discharge/charge profiles of the different cycles of Nb_2O_5@C at the current density of 3.5 A g^{-1} in PIBs.

Table S1. The fitted values of R_s and $R_{ct}+R_f$ at different voltage within the first cycle of Nb_2O_5@C in SIBs.

Voltage	R_s **(Ω)**	$R_{ct}+R_f$ **(Ω)**
OCV	3.56	12.41
Discharge to 1.5 V	3.48	12.87
Discharge to 1.0 V	3.49	12.93
Discharge to 0.5 V	3.47	12.54
Charge to 0.01 V	3.56	10.89
Charge to 1 V	3.51	8.92
Charge to 2.5 V	3.46	10.0
Charge to 3.0 V	3.34	9.5

Table S2. The fitted values of R_s and R_{ct}+R_f at different voltage within the first cycle of Nb_2O_5@C in PIBs.

Voltage	R_s (Ω)	$R_{ct} + R_f$ (Ω)
OCV	0.2	994.9
Discharge to 1.5 V	5.2	995.9
Discharge to 1.0 V	6.1	792.0
Discharge to 0.5 V	7.4	694.8
Charge to 0.01 V	1.2	566.2
Charge to 1 V	2.1	517.9
Charge to 2.5 V	0.1	495.2
Charge to 3.0 V	0.2	500.9

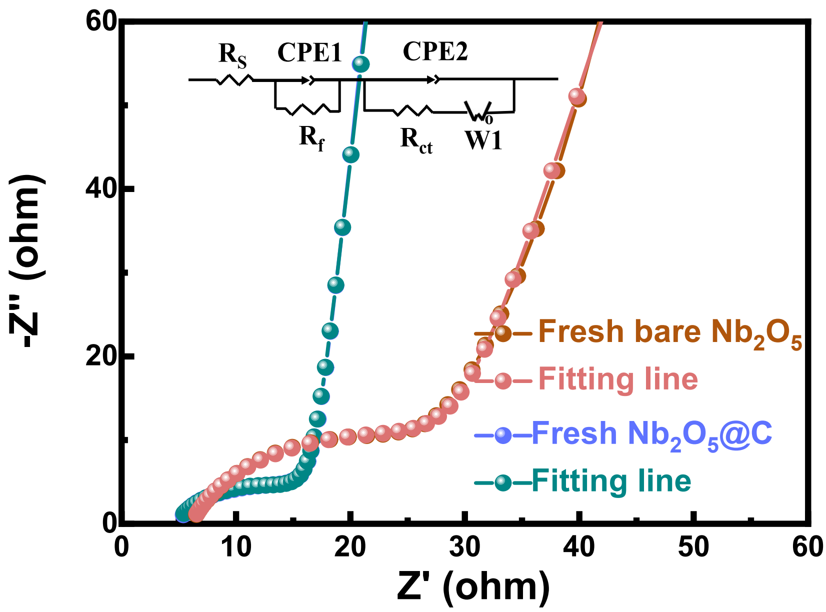

Fig. S22. The Nyquist plots of Nb_2O_5 and Nb_2O_5@C before cycling in SIBs.

Table S3. The fitted values of solution resistance (R_s) and the sum of charge transfer resistance and electrolyte/electrode interfacial resistance ($R_{ct}+R_f$) of Nb_2O_5 and Nb_2O_5@C before cycling in SIBs.

Sample	R_s **(Ω)**	$R_{ct}+R_f$ **(Ω)**
Nb_2O_5	6.11	27.76
Nb_2O_5@C	4.7	14.4

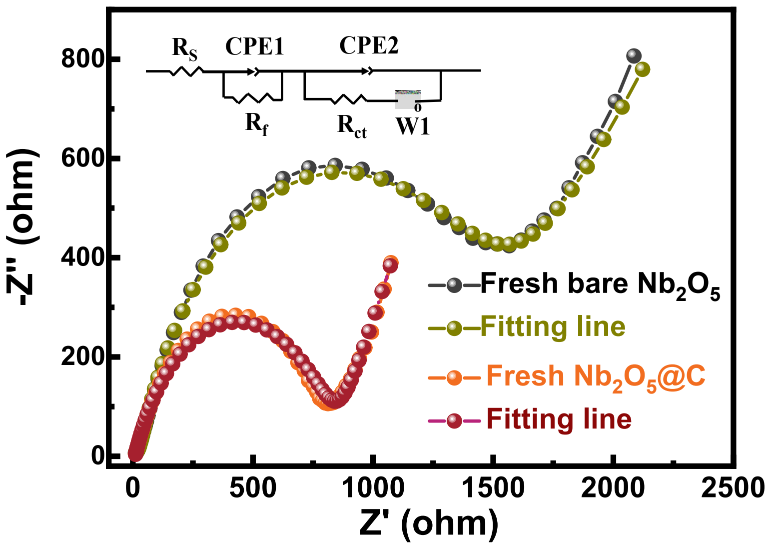

Fig. S23. The Nyquist plots of Nb_2O_5 and Nb_2O_5@C before cycling in PIBs.

Table S4. The fitted values of R_s and R_{ct}+R_f of Nb_2O_5 and Nb_2O_5@C before cycling in PIBs.

Sample	R_s **(Ω)**	R_{ct}+R_f **(Ω)**
Nb_2O_5	9.2	1393.5
Nb_2O_5@C	6.7	828.1

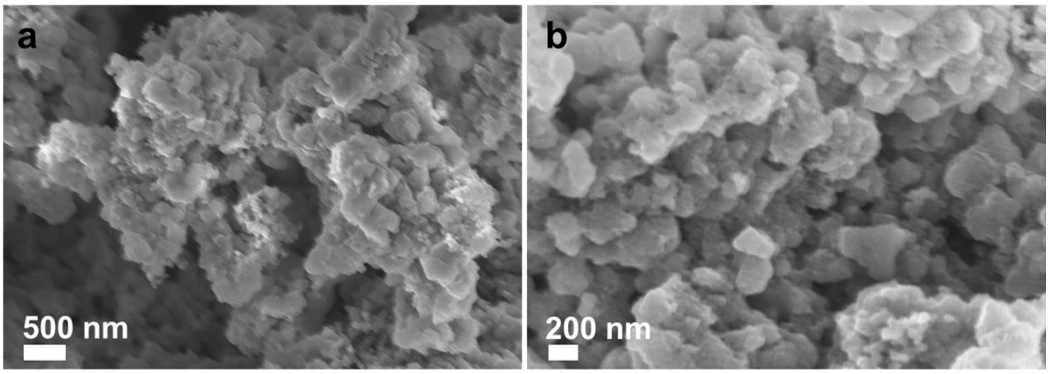

Fig. S24. (a, b) SEM images of Nb_2O_5@C tested after 200 cycles at a current density of 1 A g^{-1} in SIBs.

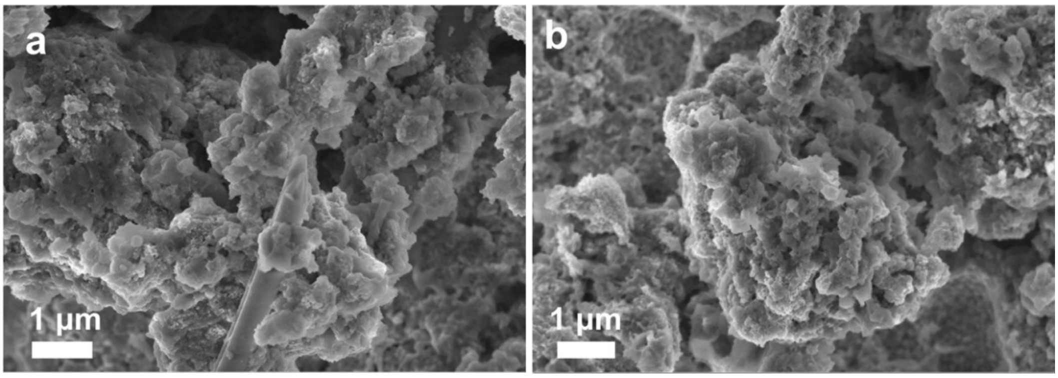

Fig. S25. (a, b) SEM images of Nb_2O_5@C tested after 500 cycles at a current density 0.5 A g^{-1} in PIBs.

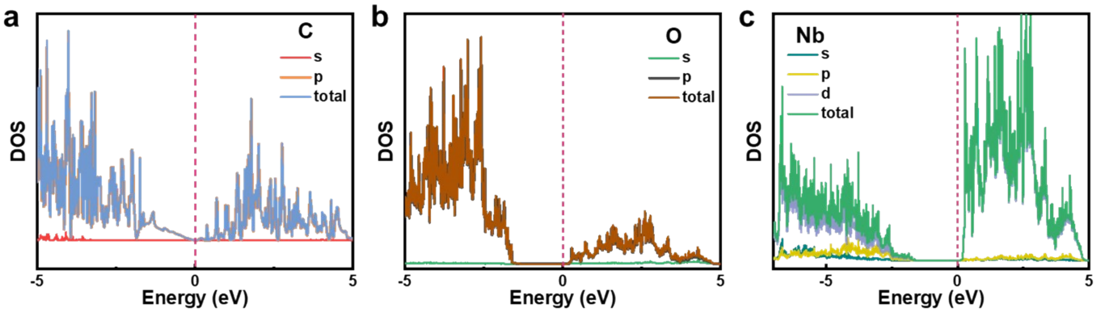

Fig. S26. The DOS of C, O and Nb.

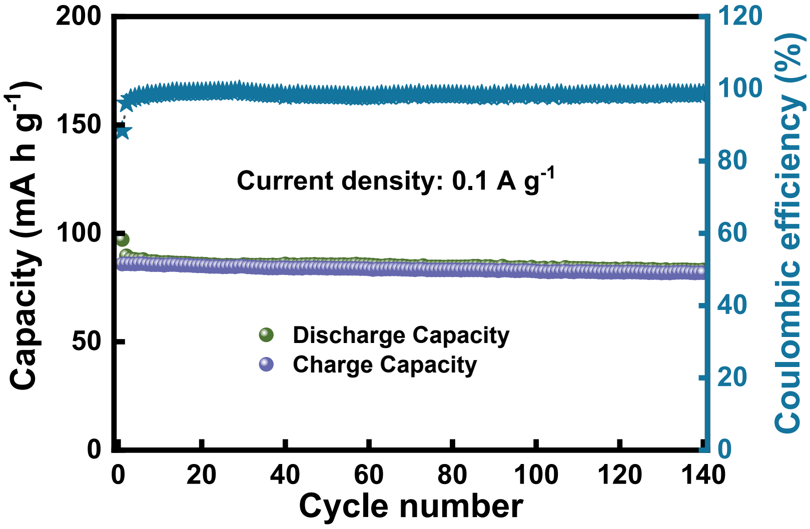

Fig. S27. The cycling performance of the commercial $Na_3V_2(PO_4)_3$ at 0.1 A g^{-1}.

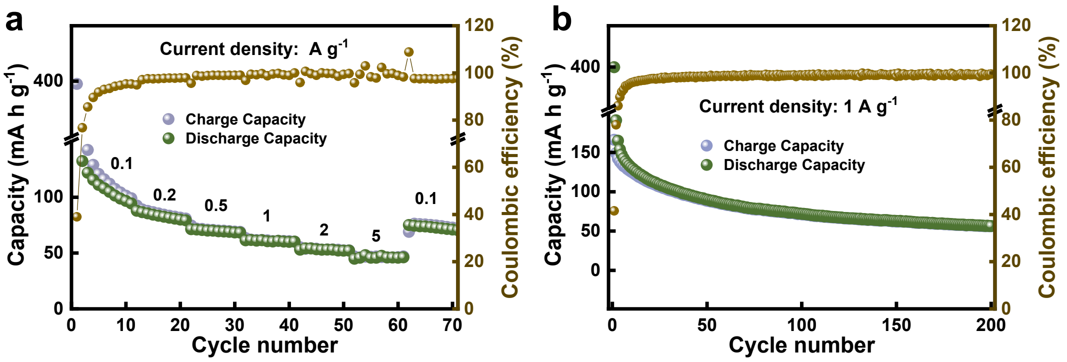

Fig. S28. (a) Rate capability and (b) cycling performance at 1 A g^{-1} of the $Na_3V_2(PO_4)_3$//Nb_2O_5@C full cell in the voltage window of 1 - 3.5 V.

Fig. S28a displays the rate performance of the $Na_3V_2(PO_4)_3$//Nb_2O_5@C full cell in a voltage window of 1 - 3.5 V, showing the capacities of 104.8, 82.5, 69.5, 60.4, 53.1, and 45.8 mA h g^{-1} at 0.1, 0.2, 0.5, 1, 2 and 5 A g^{-1}, respectively. And the capacity bounced back to 73.8 mA h g^{-1} once the current density recovered to 100 mA g^{-1}. **Fig. S28**b presents the long-term cycling performance of the full cell, which maintained a capacity of 56.8 mA h g^{-1} at 1 A g^{-1} over 200 cycles with a Coulombic efficiency closed to 100%.

Table S5. Comparison of the rate capability and cycling performance of Nb_2O_5-based composites employed as active material for sodium/potassium-ion electrodes.

Materials		Cycling performance (mA h g^{-1})	Rate Capability (mA h g^{-1})	Ref.
600-Nb_2O_5@NC-2	SIBs	278 after 100 cycles at 0.1 A g^{-1} 128 after 3000 cycles at 5 A g^{-1} 95.9 after 3000 cycles at 10 A g^{-1}	280 at 0.1 A g^{-1} 250 at 0.2 A g^{-1} 225 at 0.5 A g^{-1} 200 at 1 A g^{-1} 166 at 2 A g^{-1} 130 at 5 A g^{-1} 98 at 10 A g^{-1}	1
Nb_2O_5 NCs/rGO	SIBs	181 after 100 cycles at 0.2 A g^{-1}	195 at 0.5 A g^{-1} 170 at 1 A g^{-1} 143 at 2 A g^{-1} 115 at 5 A g^{-1} 85 at 10 A g^{-1}	2
Nb_2O_5@3D PRS	SIBs	130 after 7500 cycles at 10 C	302 at 0.5 C 265 at 1 C 240 at 2 C 225 at 3 C 202 at 5 C 176 at 8 C 158 at 10 C 140 at 15 C 126 at 20 C 108 at 25 C	3
T-Nb_2O_5/ CNF	SIBs	150 after 5000 cycles at 1 A g^{-1}	229 at 0.1 A g^{-1} 189.8 at 0.2 A g^{-1} 162.9 at 0.5 A g^{-1} 145.7 at 1 A g^{-1} 129.4 at 2 A g^{-1} 113.3 at 4 A g^{-1} 97 at 8 A g^{-1}	4

m-Nb_2O_5/C	SIBs	252 after 200 cycles at 0.05 A g^{-1} 125 after 1000 cycles at 1 A g^{-1}	252 at 0.05 A g^{-1} 123 at 1 A g^{-1} 80 at 2 A g^{-1}	5
S-Nb_2O_5 HNS@S-rGO	SIBs	215 after 100 cycles at 0.5 C 140 after 1000 cycles at 5 C 100 after 3000 cycles at 20 C	290 at 0.25 C 260 at 0.5 C 230 at 1 C 180 at 2.5 C 155 at 5 C 125 at 10 C 100 at 20 C	6
T-$Nb_2O_{5-x}F_y$∝C-NBs	SIBs	239 after 100 cycles at 0.05 A g^{-1} 130 after 10000 cycles at 1 A g^{-1}	318 at 0.025 A g^{-1} 292.2 at 0.05 A g^{-1} 264 at 0.1 A g^{-1} 230 at 0.2 A g^{-1} 194 at 0.4 A g^{-1} 178 at 0.8 A g^{-1} 165 at 1 A g^{-1} 141 at 2 A g^{-1}	7
a-H-Nb_2O_5	SIBs	133 after 1000 cycles at 2 C 109 after 3000 cycles at 5 C	185 at 0.5 C 181 at 1 C 159 at 2 C 117 at 5 C 84 at 10 C	8
m-Nb_2O_5/CNF	SIBs	190.6 after 2500 cycles at 10 C 175.8 after 3000 cycles at 5 C	286.8 at 0.5 C 282.2 at 1 C 260.1 at 2.5 C 243.9 at 5 C 224 at 10 C 196.4 at 25 C 185.6 at 50 C 178.6 at 100 C 171.4 at 150 C	9
Sb–Nb_2O_5 nanomeshes	SIBs (0.01-2 V)	190 after 500 cycles at 5 A g^{-1}	270 at 2 A g^{-1}	10

Nb_2O_5@MoS_2@C CNFs	SIBs	About 190 after 1000 cycles at 1 A g^{-1} 127 after 20000 cycles at 5 A g^{-1}	245 at 0.2 A g^{-1} 220 at 0.5 A g^{-1} 201 at 1 A g^{-1} 180 at 2 A g^{-1} 155 at 5 A g^{-1} 133 at 10 A g^{-1} 115 at 15 A g^{-1} 97 at 20 A g^{-1}	11
black Nb_2O_{5}-*x*@rGO nanosheets	SIBs	150 after 2000 cycles at 1 A g^{-1}	202 at 0.5 A g^{-1} 152 at 1.5 A g^{-1} 123 at 3 A g^{-1}	12
	PIBs	About 150 after 200 cycles at 0.2 A g^{-1} About 120 after 500 cycles at 0.5 A g^{-1} 81 after 3500 cycles at 1.5 A g^{-1}	111 at 1 A g^{-1}	
Nb_2O_5 NRs/NMMCNF	SIBs	126 after 10000 cycles at 2 A g^{-1}	275 at 0.02 A g^{-1} 101 at 4 A g^{-1}	13
T-Nb_2O_5 nanowires	PIBs	104 after 400 cycles at 0.4 A g^{-1}	152 at 0.1 A g^{-1} 127 at 0.2 A g^{-1} 104 at 0.4 A g^{-1} 90 at 0.6 A g^{-1} 81 at 0.8 A g^{-1} 74 at 1 A g^{-1}	14
Nb_2O_5@C	**SIBs**	**255 after 150 cycles at 1 A g^{-1}** **160.7 after 1000 cycles at 10 A g^{-1}**	**352.4 at 0.2 A g^{-1}** **299 at 0.5 A g^{-1}** **259 at 1 A g^{-1}** **225 at 2 A g^{-1}** **191 at 5 A g^{-1}** **163 at 10 A g^{-1}**	**This work**
	PIBs	**143 after 500 cycles at 0.5 A g^{-1}** **118 after 1600 cycles at 3.5 A g^{-1}**	**237 at 0.1 A g^{-1}** **175 at 0.2 A g^{-1}** **140 at 0.5 A g^{-1}** **114 at 1 A g^{-1}** **91 at 2 A g^{-1}**	

			70.5 at 3.5 A g^{-1} **53 at 5 A g^{-1}**	

Reference

1. Z. Chen, W. Chen, H. Wang, Z. Xiao and F. Yu, *Nanoscale*, 2020, **12**, 18673-18681.
2. L. Yan, G. Chen, S. Sarker, S. Richins, H. Wang, W. Xu, X. Rui and H. Luo, *ACS Appl. Mater. Interfaces*, 2016, **8**, 22213-22219.
3. H. Yang, R. Xu, Y. Gong, Y. Yao, L. Gu and Y. Yu, *Nano Energy*, 2018, **48**, 448-455.
4. L. Yang, Y.-E. Zhu, J. Sheng, F. Li, B. Tang, Y. Zhang and Z. Zhou, *Small*, 2017, **13**, 1702588.
5. Y. Wu, X. Fan, R. R. Gaddam, Q. Zhao, D. Yang, X. Sun, C. Wang and X. S. Zhao, *J. Power Sources*, 2018, **408**, 82-90.
6. F. Liu, X. Cheng, R. Xu, Y. Wu, Y. Jiang and Y. Yu, *Adv. Funct. Mater.*, 2018, **28**, 1800394.
7. Y. Wu, X. Fan, Y. Chen, R. R. Gaddam, F. Yu, C. Xiao, C. Lin, Q. Zhao, X. Sun, H. Wang, C. Liu, J. Li and X. S. Zhao, *J. Mater. Chem. A*, 2019, **7**, 20813-20823.
8. J. Ni, W. Wang, C. Wu, H. Liang, J. Maier, Y. Yu and L. Li, *Adv. Mater.*, 2017, **29**, 1605607.
9. Y. Li, H. Wang, L. Wang, Z. Mao, R. Wang, B. He, Y. Gong and X. Hu, *Small*, 2019, **15**, 1804539.
10. L. Wang, X. Bi and S. Yang, *J. Mater. Chem. A*, 2018, **6**, 6225-6232.
11. Q. Deng, F. Chen, S. Liu, A. Bayaguud, Y. Feng, Z. Zhang, Y. Fu, Y. Yu and C. Zhu, *Adv. Funct. Mater.*, 2020, **30**, 1908665.
12. Z. Tong, R. Yang, S. Wu, D. Shen, T. Jiao, K. Zhang, W. Zhang and C.-S. Lee, *Small*, 2019, **15**, 1901272.

13. L. She, F. Zhang, C. Jia, L. Kang, Q. Li, X. He, J. Sun, Z. Lei and Z.-H. Liu, *J. Colloid Interface Sci.*, 2020, **573**, 1-10.

14. N. Li, F. Zhang and Y. Tang, *J. Mater. Chem. A*, 2018, **6**, 17889-17895.